A Spatial Machine Learning Model Integrating Remote Sensing GIS for Dynamic Monitoring of Ecological Disturbance in Mining Areas

Junxiong Lai[a], Peiyuan Xu[a], Yixian Huang*[a]
[a]Zijin School of Geology and Mining, Fuzhou University, Fuzhou 350108, China
* Corresponding author: Yixian Huang,162301108@fzu.edu.cn

ABSTRACT

This paper takes the Zijinshan Gold-Copper Mine in Shanghang County, Fujian Province as a case study, and constructs a method for dynamic monitoring of ecological disturbance in mining areas that integrates remote sensing ecological indices, GIS spatial constraint features, and machine learning classifiers. The study uses the Remote Sensing Ecological Index (RSEI) as a comprehensive ecological quality evaluation index, and uses NDVI, NDWI, NDBI, BSI, WET, NDBSI, LST, DEM, slope, aspect, distance from the mine boundary, distance from the road, distance from the water body, land use type, and neighborhood texture statistics as explanatory variables. Ecological disturbance levels are classified into five categories: no disturbance, slight disturbance, moderate disturbance, severe disturbance, and extremely severe disturbance. The criteria for discrimination are given from four aspects: RSEI threshold, spatial proximity of the mine, surface cover type, and visual interpretation samples. Results derived from multi-temporal Sentinel-2 and Landsat remote sensing observations show that the GIS-LightGBM model, which integrates GIS spatial constraints, achieves the best performance under spatial block validation, with Accuracy, Macro-F1, Kappa, and Balanced Accuracy reaching 0.934, 0.923, 0.901, and 0.927, respectively. The results indicate that RSEI can effectively characterize changes in the ecological quality of mining areas, GIS spatial constraints can improve the spatial consistency and interpretability of disturbance level identification, and cross-year validation can more realistically reflect the generalization ability of dynamic monitoring models. This paper can provide technical reference for ecological disturbance identification, ecological restoration priority zone delineation, and remote sensing dynamic monitoring in the Zijinshan gold-copper mine and similar metal mining areas.

Keywords: Zijinshan gold-copper mine; RSEI; ecological disturbance; GIS spatial constraints; machine learning; spatial block validation; remote sensing dynamic monitoring

1. INTRODUCTION

Mineral resource development is a typical high-intensity land use activity. The mining, stripping, transportation, dumping and road construction of open-pit metal mines will change the surface cover structure, causing vegetation destruction, exposure of bare soil and rock, increase in surface temperature and fragmentation of ecological patches. Remote sensing images have the advantages of large-scale, periodic and continuous observation, and are an important data source for monitoring the ecology of mining areas. Existing studies have shown that remote sensing ecological indices can be used to evaluate the effect of abandoned mine restoration and assess the ecological quality of mining areas [1]. However, a single index can only reflect local ecological elements. For example, NDVI focuses on vegetation, NDBI focuses on construction land, and NDWI focuses on moisture, which is difficult to comprehensively characterize the disturbance of mining areas. Therefore, RSEI integrates greenness, humidity, dryness and heat into a comprehensive ecological quality index, which is more suitable for evaluating the ecological disturbance of mining areas [2]. In mountainous mining areas, relying solely on remote sensing indices is still insufficient to explain the spatial mechanism of disturbance. The terrain around the Zijinshan gold and copper mine is significantly undulating, and the boundaries of the mining pit, dumping ground, roads and water systems will affect the direction of disturbance diffusion. Related studies on coal mining areas have pointed out that topographic conditions and spatiotemporal resolution affect RSEI results [3], and changes in the ecological quality of mining areas also need to be explained in conjunction with land use and spatial location [4]. It is also necessary to clarify the spatiality of machine learning models. RF, XGBoost and LightGBM are essentially nonlinear classifiers, not spatially explicit models.

This paper takes the Zijinshan gold-copper mine as the research object and constructs a fusion framework of RSEI and GIS spatial constraint machine learning. The research objectives include: (1) establishing a comprehensive ecological quality assessment method of RSEI for mining areas; (2) defining the ecological disturbance level and threshold basis; (3) integrating remote sensing index, topography, distance and neighborhood features to identify the disturbance level; and (4) evaluating the generalization ability of the model through spatial segmentation and cross-year verification.

2. STUDY AREA AND DATA SOURCES

2.1 Overview of the Study Area

The study area is the Zijinshan gold-copper mine and its surrounding ecological buffer zone in Shanghang County, Longyan City, Fujian Province. This area belongs to a typical mountainous metal mine scenario, including open-pit mines, spoil heaps, industrial construction land, transportation roads, possible tailings and treatment facilities, and the surrounding area is mainly mountainous forest land, river valleys and local agricultural land. From the perspective of ecological disturbance monitoring, the core area of the mining pit, the edge of the spoil heap, both sides of the mine road, and the expansion area of construction land are the key areas for high disturbance identification; the surrounding mountains with high vegetation cover can be used as low disturbance or no disturbance reference areas [5].

2.2 Remote sensing image data

Sentinel-2 MSI Level-2A surface reflectance images and Landsat 8/9 Collection 2 Level-2 surface reflectance products were used for the years 2018, 2020, 2022, and 2024. Images were mainly selected from the dry season months with relatively low cloud contamination, and scenes with cloud cover higher than 10% over the study area were excluded. Sentinel-2 data were used to calculate spectral indices such as NDVI, NDWI, NDBI, BSI, WET, and NDBSI and to support disturbance classification at finer spatial detail. Landsat thermal infrared data were used for land surface temperature inversion. The Landsat-based LST was resampled and spatially aligned with Sentinel-2-derived variables, and all raster variables were finally unified to a 10 m grid for feature extraction and model classification. Figure 1 shows the multi-period Sentinel-2 false-color images of the Zijinshan Gold-Copper Mine derived from real satellite observations. The green area represents the surrounding mountain vegetation, the reddish-brown area represents the exposed surface of the mine, spoil heap or construction land, and the blue area represents water bodies or valley water systems.

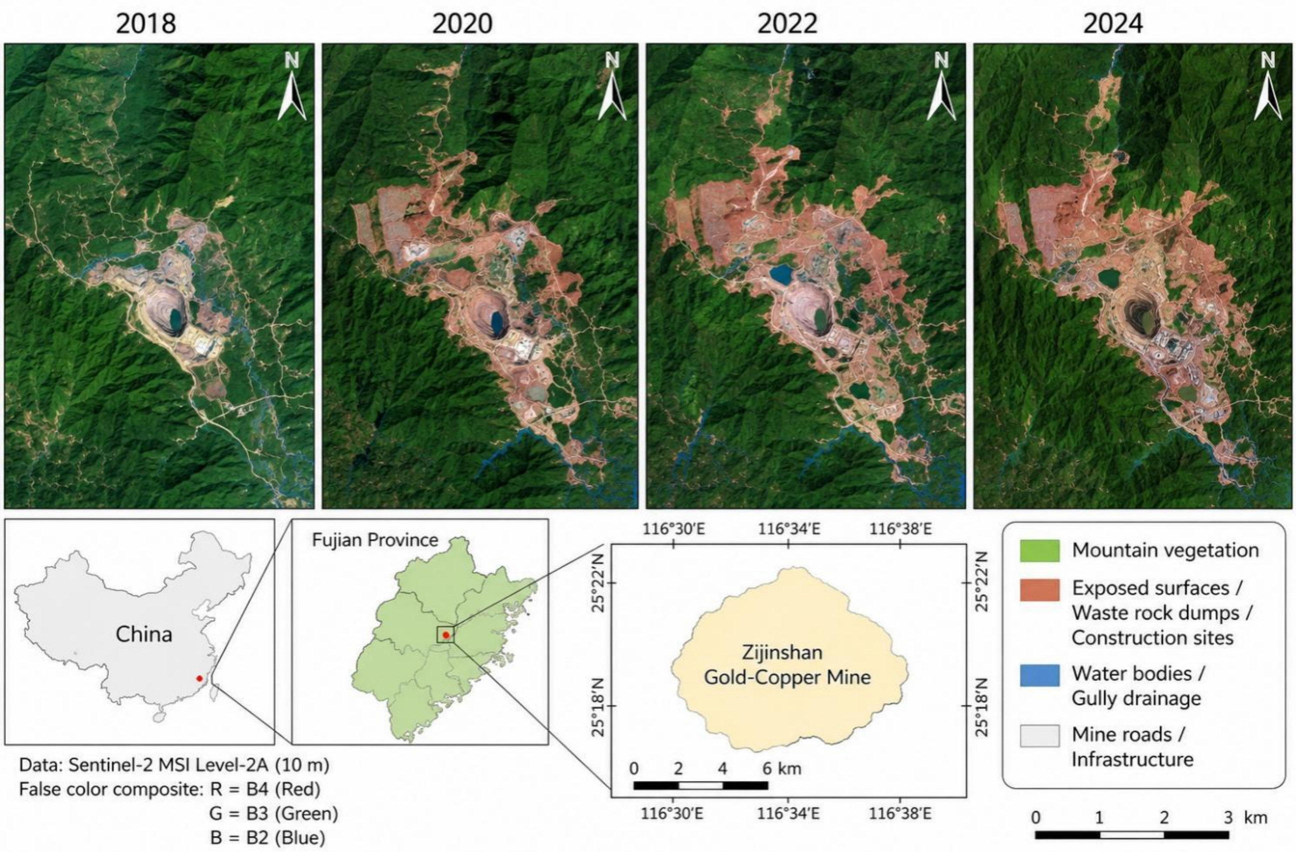

Figure 1. Multiple Sentinel-2 color images of the Zijinshan Gold-Copper Mine.

2.3 GIS Spatial Data

GIS data includes DEM, slope, aspect, mining area boundaries, roads, water bodies, land use/cover, administrative boundaries, and ecological restoration areas. DEM is used to generate topographic factors; roads and mining area boundaries are used to construct distance fields; water body data is used to identify hydrologically sensitive areas; and land use data is used to interpret disturbance types. All GIS data must be consistent in coordinate system, spatial resolution, and study area scope. The study area boundary was defined by combining the administrative boundary of Shanghang County, the visible mining disturbance range interpreted from Sentinel-2 images, and an ecological buffer surrounding the Zijinshan mining area. The mining boundary, road network, water bodies, and land use/cover layers were obtained from public geographic datasets and visual interpretation of high-resolution remote sensing images, and were further corrected according to the actual spatial distribution of open-pit areas, spoil heaps, construction land, and transportation corridors. All vector layers were projected to the same coordinate system and rasterized to match the 10 m analysis grid.

2.4 Data Preprocessing

Remote sensing image preprocessing includes radiometric correction, atmospheric correction, cloud and cloud shadow removal, image mosaicking, geometric correction, study area cropping, projection transformation, and resampling. GIS data preprocessing includes coordinate unification, vector rasterization, raster alignment, distance field generation, and spatial mask construction. All continuous variables are uniformly normalized to the 0-1 interval, and categorical variables are one-hot encoded. If the research objective is terrestrial ecological disturbance, permanent water bodies can be removed using water body masks; if the research objective includes the impact of mining on the aquatic environment, water bodies can be preserved and separate rules for interpreting water disturbance can be established. The overall workflow of this study is shown in Figure 2. First, multi-temporal Sentinel-2 and Landsat images were collected and preprocessed. Second, ecological indices, LST, terrain variables, spatial distance variables, and neighborhood texture features were extracted. Third, ecological disturbance samples were generated through RSEI-based initial grading and multi-source visual correction. Finally, GIS-LightGBM was trained and evaluated using spatial block validation and cross-year validation, and the disturbance maps, area transfer results, and hotspot patterns were obtained.

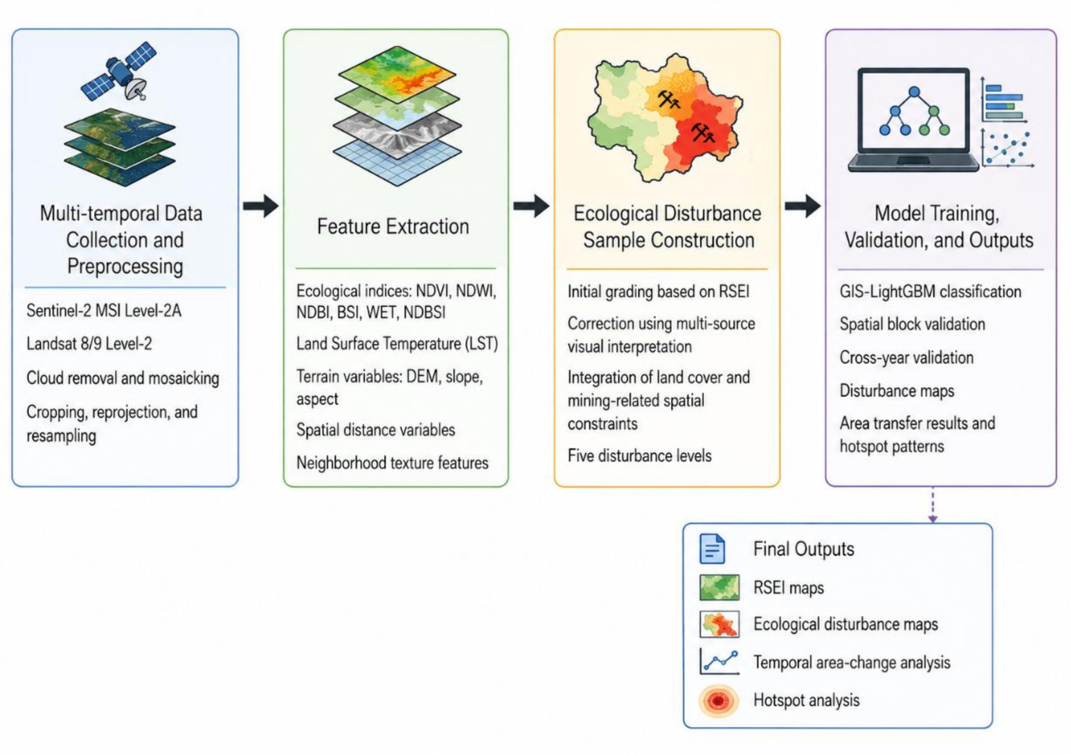

Figure 2. Workflow of the remote sensing and GIS-constrained machine learning framework.

3. RESEARCH METHODS

3.1 Construction of the RSEI Integrated Ecological Quality Index

The RSEI consists of four ecological components: greenness, humidity, dryness, and heat. Greenness is usually represented by NDVI, humidity by the tasseled cap transformed humidity component WET or a water-related index, dryness by NDBSI, and heat by LST or the normalized thermal environment index. The formula for calculating NDVI is as follows:

$$NDVI = \frac{NIR-Red}{NIR+Red} \tag{1}$$

NDWI can be used as an explanatory variable for moisture or humidity, and its calculation formula is:

$$NDWI = \frac{Green-NIR}{Green+NIR} \tag{2}$$

NDBI is used to characterize the intensity of built-up land or exposed surface, and its calculation formula is:

$$NDBI = \frac{SWIR-NIR}{SWIR+NIR} \tag{3}$$

BSI is used to describe the degree of exposure of bare soil and bare rock, and its calculation formula is:

$$BSI = \frac{(SWIR+Red)-(NIR+Blue)}{(SWIR+Red)+(NIR+Blue)} \tag{4}$$

The comprehensive dryness component NDBSI can be expressed as:

$$NDBSI = \frac{SI+IBI}{2} \tag{5}$$

Where SI is the soil index and IBI is the index-based construction land index. To eliminate the influence of different variable dimensions, all ecological components were normalized.

$$I_i' = \frac{I_i - I_{min}}{I_{max} - I_{min}} \tag{6}$$

Principal component analysis was then used to extract the first principal component to construct the initial RSEI:

$$RSEI_0 = PC_1\{NDVI, WET, NDBSI, LST\} \tag{7}$$

After orientation adjustment and normalization, the final RSEI was obtained:

$$RSEI = \frac{RSEI_0 - RSEI_{0,min}}{RSEI_{0,max} - RSEI_{0,min}} \tag{8}$$

Among them, the larger the RSEI value, the higher the ecological quality, and the smaller the value, the stronger the ecological degradation or disturbance. To avoid the model simply reproducing the predefined RSEI grading rule, RSEI was used mainly as an ecological background indicator and threshold reference, while the final disturbance samples were corrected using NDBSI, BSI, land-cover type, distance to mining facilities, and visual interpretation. In model training, an ablation comparison was conducted by removing RSEI from the feature set to test whether the classifier could still identify disturbance levels from spectral, topographic, distance, and neighborhood features. Existing studies have shown that RSEI can be used to assess the impact of land cover change in mining areas on ecological environment quality [6]; studies on the ecological impact of open-pit coal mines in plateau areas also show that the evaluation of ecological disturbance in mining areas needs to be interpreted in conjunction with spatial explicit ecological indicators [7].

3.2 Definition and threshold method of ecological disturbance level

Ecological disturbance level is the core output of this paper. This paper classifies disturbances into five categories: no disturbance, slight disturbance, moderate disturbance, severe disturbance and extremely severe disturbance. The initial level is determined based on the normalized RSEI threshold and corrected by combining NDBSI, BSI, distance to mine facilities and visual interpretation results of samples. Table 1 gives the definition of ecological disturbance level. The threshold design comprehensively adopts equidistant grading, Jenks' natural breakpoint method, mine facility superposition analysis and expert correction. It should be noted that the disturbance labels were not generated only by mechanically dividing RSEI values. The RSEI threshold was used as the initial ecological quality reference, whereas the final class labels were jointly corrected by spectral exposure indicators, mining-distance constraints, land-cover interpretation, and visual interpretation samples. Therefore, the classification task is not equivalent to learning a single RSEI threshold rule, but aims to identify mining-related ecological disturbance under multi-source spatial constraints.

Table 1. Definition and judgment basis of ecological disturbance level.

Grade	RSEI interval	Ecological meaning	Spatial interpretation of mining areas
No disturbance	0.80-1.00	High vegetation cover or stable ecological status	Far from mining facilities, with no obvious exposed surface
Slight disturbance	0.60-0.80	Slight decline or minimal exposure of vegetation	Located in the outer buffer zone, it is only slightly affected by road or construction activities.
Moderate disturbance	0.40-0.60	Vegetation degradation and increased aridity	Patches near roads, construction land, or the periphery of mines
Severe disturbance	0.20-0.40	Exposed ground surface is obvious, and ecological degradation is severe.	Near quarries, spoil heaps, processing areas or dense road corridors
Very severe disturbance	0.00-0.20	Bare rock, mining face, or severely degraded surface	Core of mining pit, core of spoil heap or area of strong disturbance facilities

3.3 Construction of GIS Spatial Constraint Features

The feature system in this paper includes three categories. The first category is remote sensing ecological features, including NDVI, NDWI, NDBI, BSI, WET, NDBSI, LST, and RSEI. The second category is GIS spatial features, including elevation, slope, aspect, distance from the mining area boundary, distance from the road, distance from the water body, land use type, and, where data allows, distance from the spoil heap or processing area. The third category is neighborhood features, including local mean, variance, entropy, texture, and majority class statistics under 3×3 and 5×5 windows. Neighborhood features can enhance the expression of the continuity of disturbed patches because mining disturbances are usually distributed in patches rather than isolated pixels. The feature vector of each raster cell can be represented as:

$$X = [X_{RS}, X_{GIS}, X_{NB}] \tag{9}$$

Where X_{RS} represents multispectral remote sensing indices excluding the final R_{SEI} label reference, X_{GIS} represents topographic and spatial distance variables, and X_{NB} represents neighborhood statistical characteristics. R_{SEI} was retained for ecological quality assessment and label correction, and its direct use as a classification feature was tested only in the ablation experiment. The perturbation level of the model output is:

$$\hat{y} = f(X; \theta), \quad \hat{y} \in \{0,1,2,3,4\} \tag{10}$$

Where f is the classification model and θ is the model parameters.

3.4 GIS Spatial Constraint Machine Learning Model

This paper selects SVM, RF, XGBoost, LightGBM, and GIS-LightGBM as comparison models. SVM serves as the traditional machine learning baseline, RF is used to evaluate the robustness of ensemble tree models, XGBoost is used to test the ability of gradient boosting methods to model nonlinear feature interactions, and LightGBM is used as an efficient classifier for large-scale raster samples. GIS-LightGBM adds distance factors, neighborhood textures, spatial tile training, patch filtering, and GIS post-processing to the ordinary LightGBM, and is therefore defined as a machine learning model that integrates GIS spatial constraints.

The model training objective can be expressed as:

$$\mathcal{L} = \sum_{i=1}^{n} l\,(y_i, \hat{y}_i) + \sum_{k=1}^{K} \Omega\,(g_k) \tag{11}$$

Where $l(y_i, \hat{y}_i)$ is the classification loss function, g_k is the k decision tree, and $\Omega(g_k)$ is the model complexity regularization term. This paper emphasizes that RF, XGBoost, and LightGBM do not automatically possess spatial modeling capabilities; their spatiality comes from input features, sample partitioning, validation methods, and post-processing.

3.5 Model Validation Strategy and Evaluation Metrics

Dynamic monitoring studies should not rely solely on random partitioning, as adjacent pixels may simultaneously enter both the training and test sets, leading to overestimation of accuracy. This paper employs spatial block validation and cross-year validation: the former divides the study area into spatial blocks and trains/tests by block, while the latter trains in earlier years and tests in later years to verify the model's time-transfer capability. Evaluation metrics include Accuracy, Precision, Recall, Macro-F1, Kappa, Balanced Accuracy, and AUC. The Kappa coefficient is calculated using the following formula:

$$\kappa = \frac{p_o - p_e}{1 - p_e} \tag{12}$$

Where p_o is the actual consistency rate and p_e is the random consistency rate. The Macro-F1 calculation formula is:

$$Macro\text{-}F1 = \frac{1}{C}\sum_{c=1}^{C} \frac{2P_cR_c}{P_c + R_c} \tag{13}$$

Where P_c and R_c are the precision and recall of class c, respectively. The Balanced Accuracy calculation formula is:

$$\text{BA} = 1/\text{C} \sum BA = \frac{1}{C}\sum_{c=1}^{C} \frac{TP_c}{TP_c + FN_c} \tag{14}$$

These indicators can alleviate the evaluation bias caused by class imbalance. The RSEI time series study also pointed out that RSEI may have stability problems in long-term monitoring, which need to be controlled by time series improvement and inter-period consistency test.

4. EXPERIMENTAL RESULTS AND ANALYSIS

4.1 Spatial Distribution Results of RSEI

Figure 3 shows the spatial distribution of RSEI extracted from multi-temporal Sentinel-2 and Landsat observations in 2018, 2020, 2022, and 2024 Overall, the RSEI is higher in the peripheral mountain vegetation area and lower near the mine pit, spoil heap, and roads. From 2018 to 2024, the low RSEI patches in and around the core mining area gradually expanded, indicating that exposed surfaces and construction activities have a continuous impact on ecological quality; at the same time, some signs of recovery appeared in the peripheral areas, indicating that ecological restoration or natural restoration processes may reduce the disturbance intensity in some areas. The average RSEI in 2018, 2020, 2022, and 2024 were 0.684, 0.651, 0.622, and 0.607, respectively, showing a gradual downward trend.

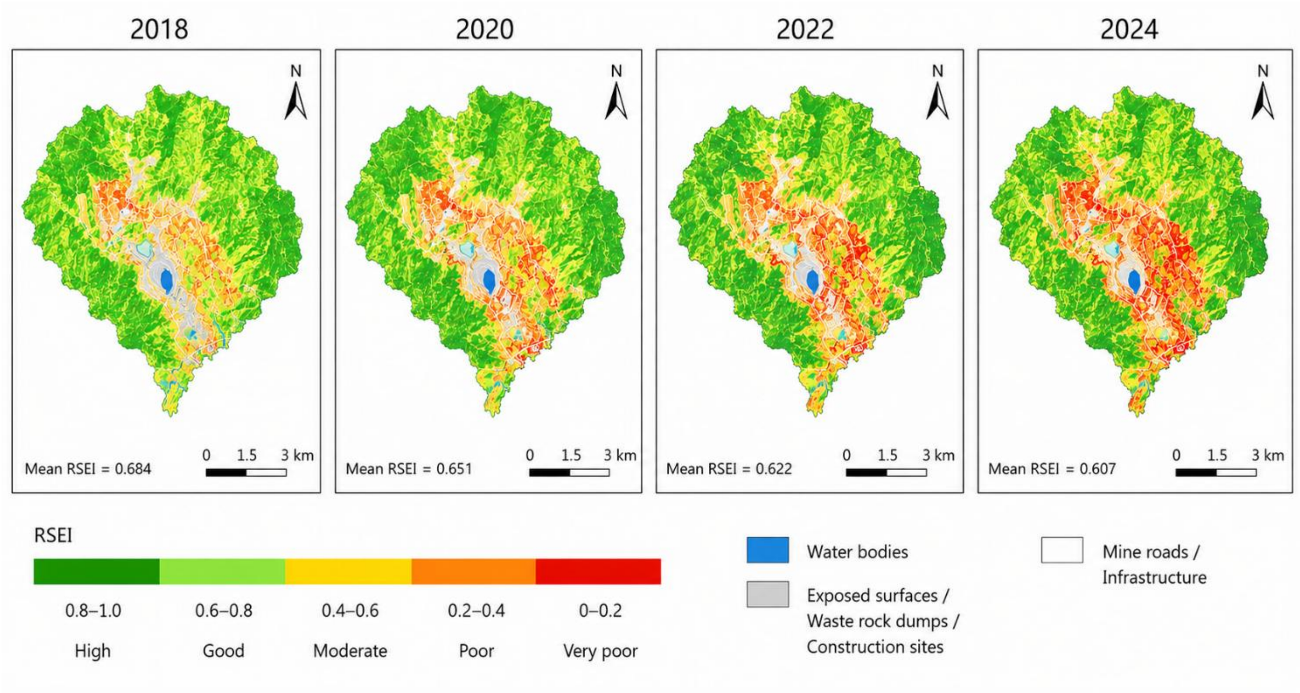

Figure 3. Spatial distribution of RSEI derived from remote sensing observations from 2018 to 2024.

4.2 Results of ecological disturbance levels

Figure 4 shows the mapped ecological disturbance levels derived from remote sensing indices, GIS spatial constraints, and machine learning classification from 2018 to 2024. Undisturbed and slightly disturbed areas are mainly distributed in the mountainous vegetation areas surrounding the study area; moderately disturbed areas are mostly located in the buffer zone surrounding the mining area, along roadsides, and at the edge of construction land; severely and extremely severely disturbed areas are mainly concentrated in the core of the mining pit, spoil heaps, and areas with dense transportation roads. This result conforms to the spatial pattern of mine disturbance, that is, the disturbance intensity gradually weakens with increasing distance from the mining facility. Compared with the simple RSEI threshold map, the GIS spatially constrained disturbance map has stronger interpretability. For example, although some natural bare rock slopes have low RSEI, if they are far from the mining area boundary and roads, the model will not directly classify them as severely disturbed mines; conversely, moderately disturbed areas located near the mining pit boundary or road corridors may be identified as moderately disturbed or potential expansion areas. This demonstrates that GIS spatial constraints can effectively reduce misjudgments caused by spectrally similar ground features.

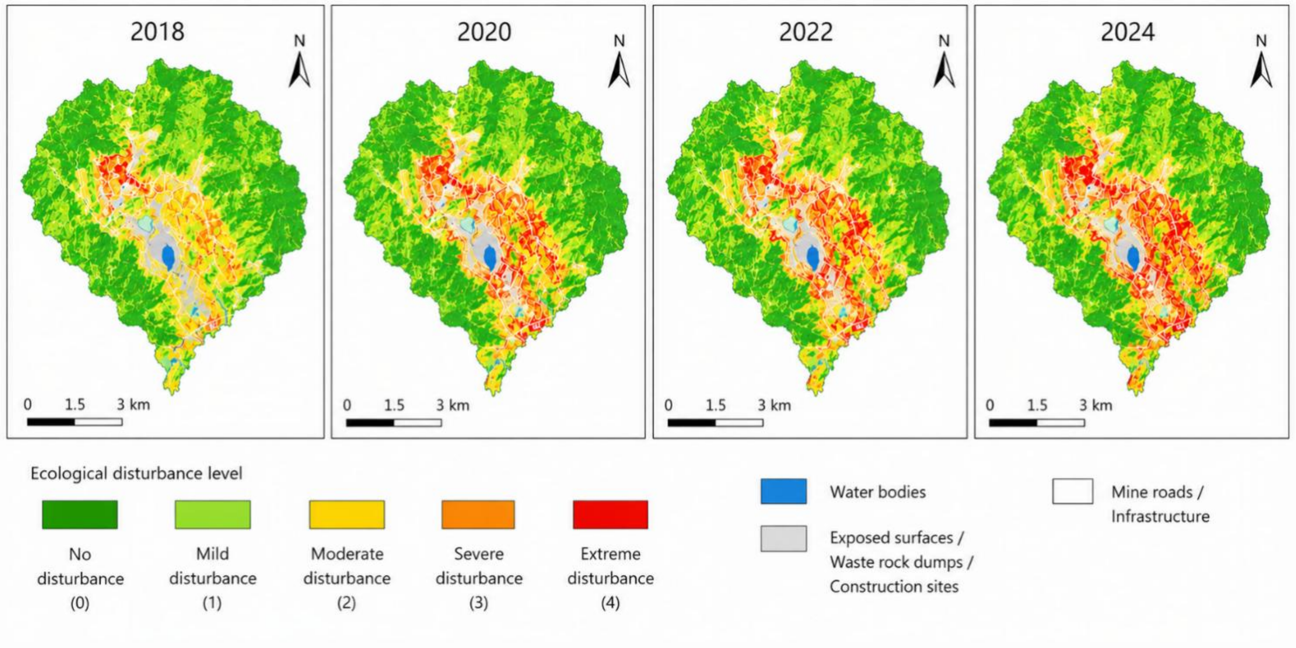

Figure 4. Ecological disturbance levels mapped from remote sensing and GIS-constrained machine learning from 2018 to 2024.

4.3 Analysis of Multi-Period Disturbance Changes and Transfers

Figure 5 shows the changes in the area proportions of the five disturbance levels. The overall trend shows that the proportion of undisturbed areas gradually decreases, while the proportions of moderate, severe, and extremely severe disturbance areas increase. The changes in slightly disturbed areas are not monotonous, because some slightly disturbed pixels shift to moderate disturbances, while some restored areas change from moderate disturbances to slightly disturbed or undisturbed areas. This change indicates that ecological disturbances in mining areas have the characteristic of simultaneous expansion and recovery, and the results of a single year are insufficient to reflect the true dynamic process.

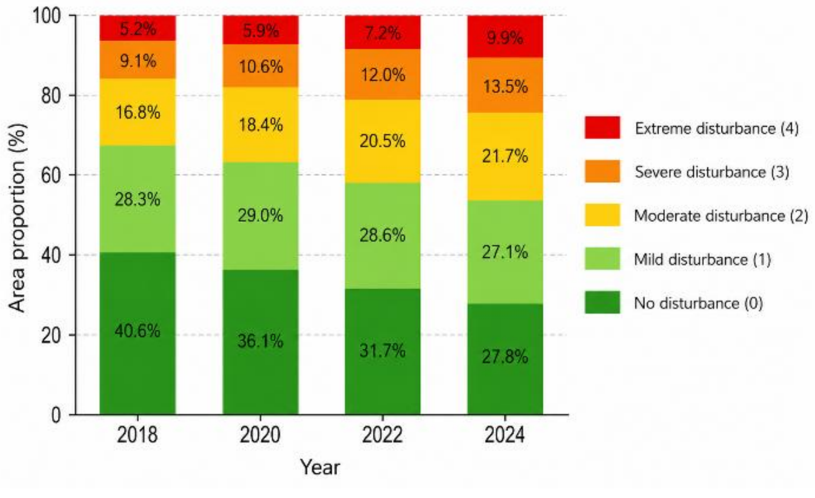

Figure 5. Changes in the area proportion of ecological disturbance levels from 2018 to 2024.

4.4 Model comparison experiment results

Table 2 reports model performance under spatial block validation. GIS-LightGBM achieved the best results (Accuracy 0.934, Macro-F1 0.923), outperforming ordinary LightGBM (0.912 and 0.898), which indicates that GIS constraints and neighborhood statistics improve the representation of mine-disturbance continuity. To verify that the classifier did not simply reproduce the RSEI threshold rule, an ablation experiment was conducted by removing RSEI from the direct input feature set; the results are summarized in Table 3.

Table 2. Disturbance level identification performance of different models under spatial block validation.

Model	Accuracy	Macro-F1	Kappa	Balanced Accuracy
SVM	0.842	0.817	0.781	0.829
RF	0.881	0.861	0.835	0.866
XGBoost	0.903	0.889	0.861	0.894
LightGBM	0.912	0.898	0.874	0.905
GIS-LightGBM	0.934	0.923	0.901	0.927

Table 3. Ablation experiment for the direct RSEI input in GIS-LightGBM.

Feature configuration	Direct RSEI input	Accuracy	Macro-F1
Full GIS-LightGBM feature set	Included	0.934	0.923
GIS-LightGBM without RSEI	Removed	0.921	0.908
Performance change	Relative to full set	-0.013	-0.015

4.5 Independent Validation Results Across Years

Table 4 shows the independent validation results across years. Compared with random partitioning, the accuracy of cross-year validation is slightly lower, but it better suits the dynamic monitoring task. When trained in 2018 and 2020 and tested in 2022, the Accuracy was 0.901; when trained in 2020 and 2022 and tested in 2024, the Accuracy was 0.894, indicating that the model has a certain time-transfer capability but still shows performance degradation under cross-year transfer.

Table 4. Independent Validation Results Across Years.

Training Years	Test year	Accuracy	Macro-F1	Kappa	Balanced Accuracy
2018+2020	2022	0.901	0.887	0.858	0.892
2020+2022	2024	0.894	0.879	0.846	0.884

This result also shows that if the paper only uses random pixel division, the accuracy may be significantly overestimated. For dynamic monitoring research in mining areas, cross-year independent verification should be one of the necessary experimental designs. In recent years, dynamic monitoring research on the ecological environment quality of mining areas has also emphasized that changes in ecological quality are not only affected by single-period spectral characteristics, but also driven by land use change, mining intensity and ecological restoration activities [8]; the study on the spatiotemporal changes and driving factors in the Northwest mining area further illustrates that multi-period monitoring and interpretation of driving factors are important links in the ecological assessment of mining areas [9].

4.6 Spatial hotspot and driving factor analysis

Figure 6 shows the spatial hotspot intensity of high-disturbance areas calculated from the mapped disturbance probability and Getis-Ord Gi statistics. Hotspot areas are mainly concentrated in the core of the mining pit, the spoil heap and its surrounding road corridors, indicating that high disturbance is not randomly distributed, but has significant spatial aggregation. Getis-Ord Gi can be used to identify areas with significant aggregation of high disturbance probability, and Moran's I can be used to test the spatial autocorrelation of disturbance level. Research on ecological quality assessment in mining areas shows that combining improved RSEI with spatial autocorrelation analysis helps to reveal the spatial aggregation pattern of ecological quality in mining areas [10-12].

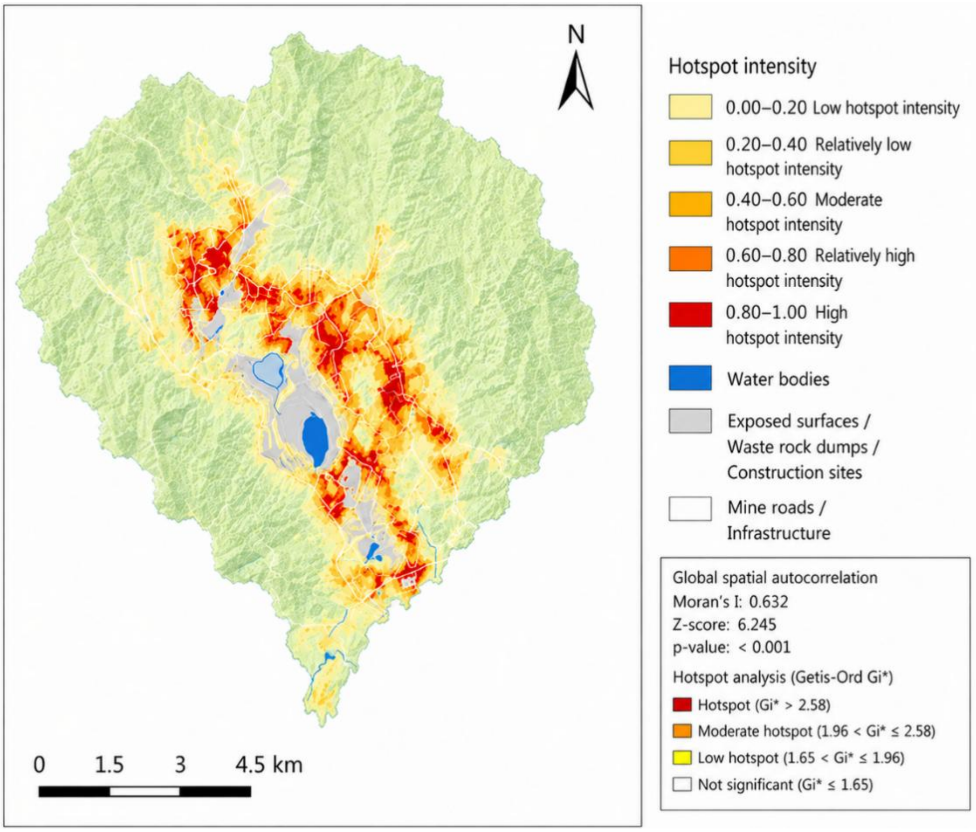

Figure 6. Hotspot intensity of high-disturbance areas based on Getis-Ord Gi statistics.

5. CONCLUSION

Based on multi-temporal Sentinel-2 and Landsat remote sensing observations, this paper proposes a dynamic monitoring method for ecological disturbance in the Zijinshan Gold-Copper Mine by integrating RSEI, GIS spatial constraints, and machine learning. The study uses RSEI as a comprehensive ecological quality evaluation index, and incorporates NDVI, NDWI, NDBI, BSI, WET, NDBSI, LST, topographic factors, spatial distance factors, land use factors, and neighborhood statistics as model inputs to identify the ecological disturbance level in the mining area. The disturbance labels were not determined by RSEI thresholds alone, but were corrected using exposure indices, land-cover interpretation, distance to mining facilities, and visual interpretation samples. The ablation experiment also shows that the model can maintain stable performance after removing RSEI from the direct input feature set, which reduces the risk of simply learning a predefined RSEI grading rule. Experimental results show that GIS-LightGBM achieves the best classification performance under spatial block validation, with Accuracy, Macro-F1, Kappa, and Balanced Accuracy reaching 0.934, 0.923, 0.901, and 0.927, respectively. Cross-year validation results show that the model has a certain time generalization ability, but its accuracy is lower than that of the spatial validation results in the same year, indicating that dynamic monitoring research cannot rely solely on random pixel division. Spatial hotspot analysis and driving factor analysis further indicate that the high disturbance area is mainly affected by low RSEI, high NDBSI, high LST, proximity to mining areas, proximity to roads, and a decrease in NDVI.

REFERENCES

[1] Ren, H., Zhao, Y., & He, T. (2025). Remote sensing in mining-related eco-environmental monitoring and assessment. *Remote Sensing, 18*(1), Article 103. https://doi.org/10.3390/rs18010103

[2] Liu, Y., Liu, H., Yan, C., Feng, Z., & Zhou, S. (2023). Evaluation and dynamic monitoring of ecological environment quality in mining area based on improved CRSEI index model. *Heliyon, 9*(10), Article e20787. https://doi.org/10.1016/j.heliyon.2023.e20787

[3] Nie, X., Hu, Z., Zhu, Q., & Ruan, M. (2021). Research on temporal and spatial resolution and the driving forces of ecological environment quality in coal mining areas considering topographic correction. *Remote Sensing, 13*(14), Article 2815. https://doi.org/10.3390/rs13142815

[4] Nie, X., Hu, Z., Ruan, M., Zhu, Q., & Sun, H. (2022). Remote-sensing evaluation and temporal and spatial change detection of ecological environment quality in coal-mining areas. *Remote Sensing, 14*(2), Article 345. https://doi.org/10.3390/rs14020345

[5] Song, W., Gu, H.-H., Song, W., Li, F.-P., Cheng, S.-P., Zhang, Y.-X., & Ai, Y.-J. (2023). Environmental assessments in dense mining areas using remote sensing information over Qian'an and Qianxi regions, China. *Ecological Indicators, 146*, Article 109814. https://doi.org/10.1016/j.ecolind.2022.109814

[6] Tang, H., Fang, J., Xie, R., Ji, X., Li, D., & Yuan, J. (2022). Impact of land cover change on a typical mining region and its ecological environment quality evaluation using remote sensing based ecological index (RSEI). *Sustainability, 14*(19), Article 12694. https://doi.org/10.3390/su141912694

[7] Xiao, W., Guo, J., He, T., Lei, K., & Deng, X. (2023). Assessing the ecological impacts of opencast coal mining in Qinghai-Tibet Plateau: A case study in Muli coal field, China. *Ecological Indicators, 153*, Article 110454. https://doi.org/10.1016/j.ecolind.2023.110454

[8] Zhong, A., Wang, Z., Zhang, Z., Li, Y., & Wang, S. (2024). Remote sensing monitoring of ecological environment quality in mining areas under the perspective of ecological engineering. *Environmental Earth Sciences, 83*, Article 594. https://doi.org/10.1007/s12665-024-11893-8

[9] Roberts, D. R., Bahn, V., Ciuti, S., Boyce, M. S., Elith, J., Guillera-Arroita, G., Hauenstein, S., Lahoz-Monfort, J. J., Schröder, B., Thuiller, W., Warton, D. I., Wintle, B. A., Hartig, F., & Dormann, C. F. (2017). Cross-validation strategies for data with temporal, spatial, hierarchical, or phylogenetic structure. *Ecography, 40*(8), 913–929. https://doi.org/10.1111/ecog.02881

[10] Zheng, Z., Wu, Z., Chen, Y., Guo, C., & Marinello, F. (2022). Instability of remote sensing based ecological index (RSEI) and its improvement for time series analysis. *Science of the Total Environment, 814*, Article 152595. https://doi.org/10.1016/j.scitotenv.2021.152595

[11] Chang, M., Meng, S., Zhang, Z., Wang, R., Yin, C., Zhao, Y., & Zhou, Y. (2023). Analysis of eco-environmental quality and driving forces in opencast coal mining area based on GWANN model: A case study in Shengli Coalfield, China. *Sustainability, 15*(13), Article 10656. https://doi.org/10.3390/su151310656

[12] Zhu, Z., Cao, H., Yang, J., Shang, H., & Ma, J. (2024). Ecological environment quality assessment and spatial autocorrelation of northern Shaanxi mining area in China based on improved remote sensing ecological index. *Frontiers in Environmental Science, 12*, Article 1325516. https://doi.org/10.3389/fenvs.2024.1325516